

Safe Multiquadcopter System Continuum Deformation Over Moving Frames

Hossein Rastgoftar D, Ella M. Atkins D, Senior Member, IEEE, and Dimitra Panagou D, Member, IEEE

Abstract—This paper proposes a new scalable model for coordination of multiple quadcopter systems by treating collective motion as continuum deformation over a moving frame. The quadcopters are considered as particles in a 2-D deformable body evolving in a 3-D motion space. The 2-D continuum reference frame (CRF) can arbitrarily translate and rotate in a 3-D motion space for maneuverability. Furthermore, a quadcopter team can significantly deform over the CRF presenting risk of interagent collisions. The formulation is therefore proven in this paper to guarantee interagent collision avoidance and quadcopter containment. Quadcopter team deformation is guided by $N_L > 3$ leader quadcopters initially placed at the vertices of a convex polygon denoted as a leading convex polygon. The CRF is then assigned based on independent leader quadcopters' 3-D positions defined by a homogeneous deformation, which, in turn, dictates follower motions. A local communication protocol is defined for the followers to acquire the desired continuum deformation. By formal characterization of the leading convex polygon deformation, both interagent collision avoidance and quadcopter containment are guaranteed in a large-scale continuum deformation coordination. A quadcopter team with 40 agents is simulated to illustrate a large-scale collective descent defined by continuum deformation coordination over a reference frame moving in the longitudinal plane.

Index Terms—Continuum deformation, local communication, multiquadcopter system, nonlinear control.

I. INTRODUCTION

ULTIAGENT SYSTEM (MAS) cooperative control has received considerable attention over the past two decades. Cooperation in an MAS allows the system to be resilient and robust in the face of disaster zone uncertainties training to understand and use. MAS cooperation can increase robustness to failure [1] and reduce total mission cost [2]. Numerous applications such as surveillance [3], traffic management [4], formation flight [5], and connected vehicle control [6], [7] have been proposed. This paper derives a continuum deformation formulation for a multiquadcopter system over a moving (translating and rotating) frame in a 3-D motion space. Mathematical

Manuscript received July 16, 2018; revised July 29, 2018 and August 1, 2018; accepted September 22, 2018. Date of publication October 4, 2018; date of current version May 28, 2019. This work was supported in part by National Science Foundation (NSF) under Grant CNS 1739525. Recommended by Associate Editor Y. Paschalidis. (Corresponding author: Hossein Rastgoftar.)

The authors are with the Department of Aerospace Engineering, University of Michigan, Ann Arbor, MI 48109 USA (e-mail: hosseinr@umich.edu; ematkins@umich.edu; dpanagou@umich.edu).

Digital Object Identifier 10.1109/TCNS.2018.2873204

guarantees are derived to achieve and maintain a prescribed continuum deformation with 3-D collision avoidance.

A. Background

Virtual structure [8], [9]; consensus [10]–[16]; containment control [17]-[19]; and continuum deformation [20]-[22] offer distributed control for MAS. The virtual structure is a centralized approach for the multiagent coordination, while the other listed approaches are decentralized. In a virtual structure, each agent's desired position can be expressed by the vector sum of two position vectors: 1) a center point (CP) position vector, for example, the MAS center of mass, and 2) a relative displacement vector with respect to the CP [8]. If the agents' relative distances from the CP remain constant, the MAS is treated as a rigid body [23]. A flexible virtual structure formation control is also studied in [24]. Virtual structure formation control is achieved with outerloop and inner-loop trajectory tracking modules. The outer-loop controller is responsible for the CP (reference) desired trajectory tracking. The inner-loop controller of each individual agent regulates relative distance from the CP.

Consensus is the most commonly applied decentralized cooperative control technique with applications including motion control [11], [12]; smart grid and power systems [13], [25]; medical applications [14]; and distributed sensing [15], [16]. A leaderless consensus control approach is applied for agent coordination in [26] and [27]. Multiagent consensus guided by a single leader is studied in [28] and [29]. In addition, an adaptive leader–follower consensus coordination, defined by a switching communication, is proposed and validated in simulation in [30].

Containment control [31] is a leader–follower method in which collective motion is guided by multiple leaders, and follower agents acquire the desired positions, defined by the containment protocol, through local communication with inneighbor agents. MAS containment control can be modeled by single and double integrator dynamics as in [31] and [32]. Containment control of higher-order MAS in which follower agents are modeled by linear dynamics is presented in [33] and [34]. Wang *et al.* [32], [35] studied the finite time containment control of second-order MAS, while MASs with switching communication topologies are studied in [36].

The authors have proposed a novel continuum deformation approach for the collective motion of MAS [20], [21]. In mechanics, a continuum (or deformable body) is a continuous domain in a 3-D space containing an infinite number of particles

with infinitesimal size [37]. A continuum deformation is a homeomorphic mapping between initial and current configurations of the continuum. Using continuum deformation, global coordination in a 3-D motion space is achieved over a class of nonsingular deformation mappings called homoeneous transformations or homogeneous deformations. Under a homogeneous deformation, agents are treated as particles of an n-D (n = 1, 2, 3)deformable body and can be classified as leaders and followers. A homogeneous transformation can be uniquely defined based on positions of n+1 leaders placed at the vertices of an n-D polytope at any time. For example, a 2-D homogeneous transformation is defined by three leaders forming a triangle. A 3-D homogeneous transformation can also be defined by four leaders at the vertices of a tetrahedron. Follower agents, located inside the convex hull defined by the leaders, acquire a global homogeneous transformation with only local interagent communication [20], [22]; potentially no interagent communication [20]; or by sensing other agents [20]. In addition, Zhao et al. [38] showed how an n-dimensional homogeneous transformation can be acquired through local communication defined by a weighted and undirected graph having a symmetric Laplacian matrix. In [38], communication weights are not restricted to be non-negative.

Like the virtual structure, a continuum deformation specifies a deformable body enclosing all agents, for example, the leading polytope defined by n+1 leaders in \mathbb{R}^n can be considered a deformable virtual structure. Therefore, interagent distances can significantly change in an agent coordination task similar to the virtual structure. A continuum deformation can be acquired by followers in real time, which can considerably reduce computational overhead in an agent-coordination scenario. Consensus and containment control are also decentralized approaches offering real-time coordination at low computational costs similar to continuum deformation.

Interagent and obstacle collision avoidance are two major challenges in multiagent coordination. By constructing appropriate distributed potential functions [39], both consensus and containment control offer interagent collision avoidance. MAS containment is another key issue. It has been proven that followers of MAS evolving under containment control eventually converge inside a convex hull defined by the leaders [40]. However, followers may leave the containment region prescribed by the leaders during evolution, which can result in interagent collision and collision with obstacles in the environment [21]. By applying continuum deformation, the authors have proven both transient containment and interagent collision avoidance during MAS evolution [20], [41].

MAS rigidity is the other key issue. When an MAS applies consensus for motion-control applications, interagent distances asymptotically converge to constant values. This can result in rigidity of the desired formation. Therefore, collective MAS motion may be difficult to analyze when MAS passage through a narrow channel is required. By applying continuum deformation, the MAS can deform as needed because interagent distances are allowed to change.

In summary, continuum deformation and containment cooperative control approaches have the following features in common: 1) they are both leader-follower methods; 2) leaders evolve independently in both continuum deformation and containment control approaches; and 3) followers acquire desired global coordination through local communication. Continuum deformation extends available containment control theory through formal support for and characterization of nontrivial deformation of the convex hull defined by leaders. Because interagent distances can significantly change and the convex hull can deform and rotate in a continuum deformation, interagent collision avoidance must be guaranteed. The continuum deformation coordination approach provides interagent collision-avoidance guarantee conditions by 1) assigning a lower-bound for deformation and 2) defining communication weights as fixed distance ratios at initial time t_0 . In addition, a multiple quadcopter continuum deformation allows navigation in constrained environments such as a narrow channel.

B. Objectives and Outline

This paper advances our previous contributions in continuum deformation of single/double integrator MAS over a stationary frame to achieve continuum deformation of a multiquadcopter system over a moving (translating and rotating) reference frame. Each quadcopter applies an input—output (IO) feedback linearization controller to asymptotically track the desired trajectory given by a continuum deformation. Compared to the available literature and the authors' previous work, this paper offers the following contributions.

- Continuum deformation over a moving frame allows significant rotation of the convex hull defined by leader quadcopters in a 3-D motion space. Therefore, maneuverability of a quadcopter team is improved.
- 2) We provide guarantee conditions on interagent collision avoidance and agent containment when the convex hull defined by leaders significantly deforms and rotates. To this end, we assign a lower bound on eigenvalues of the continuum deformation Jacobian matrix given: 1) initial agent displacement; 2) agent body size; and 3) an upper bound on the quadcopter position control error. By defining a convex prism containing the quadcopters at all times *t*, collision avoidance with obstacles in the workspace can be guaranteed.
- 3) We relax the previous constraint on the number of leaders (three) guiding a 2-D continuum deformation coordination. We show that $N_L \geq 3$ primary and secondary leaders can guide quadcopter team collective motion. Continuum deformation coordination is defined by three primary leaders. Continuum deformation coordination can be acquired by followers and secondary leaders in real time through local communication.

This paper is organized as follows. Preliminary notions on graph theory, position notations, a background on the MAS continuum deformation, and further motivation for continuum deformation coordination are presented in Section II. A problem statement in Section III is followed by specification of continuum deformation over a moving frame in a 3-D workspace (see Section IV). Quadcopter team collective motion, defined by continuum deformation over a moving frame, is mathematically

formulated in Section V. Section VI provides guarantees on interagent collision avoidance and quadcopter containment in large-scale continuum deformation coordination. Simulation results presented in Section VII are followed by concluding remarks in Section VIII.

II. PRELIMINARIES

A. Notions on Graph Theory

Let $\mathcal{G} = \mathcal{G}(\mathcal{V}, \mathcal{E}, \mathbf{W})$ be a directed graph defining interagent communication for a multiquadcopter system with node set \mathcal{V} , edge set \mathcal{E} , and weight matrix $\mathbf{W} = [W_{ij}]$. The quadcopter team consists of N vehicles moving in a 3-D motion space. Nodes of the graph are defined by the set $\mathcal{V} = \{1, 2, \dots, N\}$. Quadcopters are categorized as leaders and followers. Leader index numbers are defined by the set $\mathcal{V}_L = \{1, \dots, N_L\}$. This paper assumes that $N_L \geq 3$ leaders form a convex polygon in a 3-D motion space, for example, a convex polygon defined by leaders is called the *leading polygon*. Follower index numbers are defined by the set $\mathcal{V}_F = \mathcal{V} \setminus \mathcal{V}_L = \{N_L + 1, \dots, N\}$. Edges of graph \mathcal{G} are defined by $\mathcal{E} \subset \mathcal{V} \times \mathcal{V}$. If quadcopter $i \in \mathcal{V}_F$ updates its position based on the position of vehicle $j \in \mathcal{V}$, then $(j,i) \in \mathcal{E}$. The set $\mathcal{N}_i = \{j | i \in \mathcal{V}_F \land (j,i) \in \mathcal{E}\}$ is called the *in-neighbor set* of follower i.

Matrix $\mathbf{W} \in \mathbb{R}^{N \times N}$ specifies quadcopter communication weights. Let $w_{i,j}$ denote the communication weight of quadcopter $i \in \mathcal{V}_F$ with quadcopter $j \in \mathcal{V}$. Then, \mathbf{W} is defined by

$$\mathbf{W}_{ij} = \begin{cases} w_{i,j} & i \in \mathcal{V}_F, j \in \mathcal{N}_i \\ -1 & j = i \\ 0 & \text{else} \end{cases}$$
 (1)

Weight matrix W can be partitioned as

$$\mathbf{W} = \begin{bmatrix} -\mathbf{I} & \mathbf{0} \\ \mathbf{\Omega} & \mathbf{L} \end{bmatrix} \tag{2}$$

where $\mathbf{I} \in \mathbb{R}^{N_L \times N_L}$ is the identity matrix and $\mathbf{0} \in \mathbb{R}^{N_L \times (N-N_L)}$ is the zero-entry matrix, $\mathbf{\Omega} \in \mathbb{R}^{(N-N_L) \times N_L}$ is the follower–leader communication matrix (or FL communication matrix), and $\mathbf{L} \in \mathbb{R}^{(N-N_L) \times (N-N_L)}$ is the follower-follower communication matrix (or FF communication matrix).

B. Position Terminology

Throughout this paper, position is expressed with respect to an inertial or *ground coordinate system*. Orthogonal bases of the ground coordinate frame are denoted as $\hat{\mathbf{e}}_x$, $\hat{\mathbf{e}}_y$, and $\hat{\mathbf{e}}_z$. The *actual position* of a quadcopter $i \in \mathcal{V}$ is expressed with respect to the ground frame by

$$\mathbf{r}_i = x_i \hat{\mathbf{e}}_x + y_i \hat{\mathbf{e}}_y + z_i \hat{\mathbf{e}}_z. \tag{3}$$

The *initial position* of quadcopter $i \in \mathcal{V}$ is denoted by

$$\mathbf{r}_{i,0} = x_{i,0}\hat{\mathbf{e}}_x + y_{i,0}\hat{\mathbf{e}}_y + z_{i,0}\hat{\mathbf{e}}_z = x_i(t_0)\hat{\mathbf{e}}_x + y_i(t_0)\hat{\mathbf{e}}_y + z_i(t_0)\hat{\mathbf{e}}_z$$
(4)

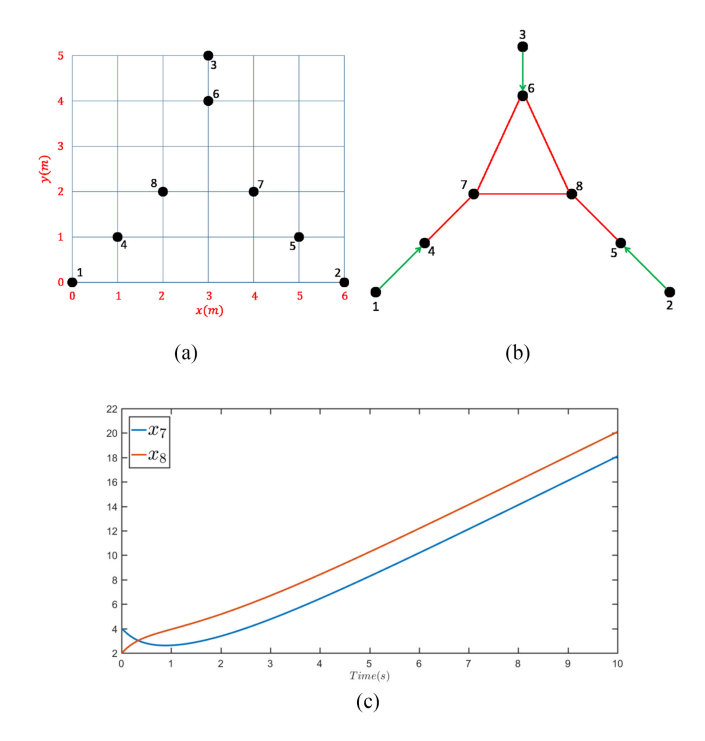


Fig. 1. (a) Initial formation of an MAS in the xy plane. Agents 1, 2, and 3 are leaders and the remaining agents are followers. (b) Typical communication graph used by followers to acquire a collective motion through local communication. (c) x components of follower agents 7 and 8 versus time.

where t_0 is the initial time. Each quadcopter i in the MAS is positioned with respect to a *global desired position*, denoted as $\mathbf{r}_{i,HT}$, as defined by a homogeneous transformation

$$i \in \mathcal{V}, \qquad \mathbf{r}_{i,HT} = \mathbf{Q}(t, t_0)\mathbf{r}_{i,0} + \mathbf{d}(t, t_0)$$
 (5)

where $\mathbf{Q} = [Q_{ij}] \in \mathbb{R}^{3 \times 3}$ is the Jacobian matrix and $\mathbf{d} = [d_i] \in \mathbb{R}^{3 \times 1}$ is the rigid body displacement vector.

Quadcopter i's local desired position is denoted by

$$\mathbf{r}_{d,i} = \begin{cases} \mathbf{r}_{i,HT} & i \in \mathcal{V}_L \\ w_{i,j}\mathbf{r}_j & i \in \mathcal{V}_F, j \in \mathcal{N}_i \end{cases}$$
(6)

Note that $w_{i,j}$ is positive and $\sum_{j\in\mathcal{N}_i} w_{i,j} = 1$. This paper assumes that the actual, local desired, and global desired positions of all agents are the same at initial time t_0 : $\mathbf{r}_{i,0} = \mathbf{r}_{i,HT}(t_0) = \mathbf{r}_{d,i}(t_0)(\forall i\in\mathcal{V})$.

C. Why Continuum Deformation?

For continuum deformation, communication weights of an individual follower are consistent with agents' initial positions. While this property of a homogeneous transformation may seem limiting, it is actually beneficial for safety in a large-scale team. This statement is supported by the example in Fig. 1. The MAS with initial formation shown in Fig. 1(a) is directed to move collectively from left to right. Using containment control, the MAS is guided by leaders 1, 2, and 3 moving on straight paths with the same constant velocity. Followers use the graph shown in Fig. 1(b) to acquire the desired collective motion through local communication. Assuming single integrator followers, follower

i updates its position by

$$\dot{\mathbf{r}}_i = \sum_{j \in N_i} gw_{i,j} \left(\mathbf{r}_j - \mathbf{r}_i \right)$$

where g=2 and follower communication weights are as follows: $w_{4,1}=w_{4,7}=w_{5,2}=w_{5,8}=0.5, w_{6,3}=\frac{2}{3}, w_{6,7}=w_{6,8}=\frac{1}{6}, w_{7,4}=w_{8,5}=0.57, w_{7,6}=w_{8,6}=0.29, w_{7,8}=w_{8,7}=0.14.$

Fig. 1(c) shows the x components of followers 7 and 8 versus time. Because leaders move horizontally, the y component of every agent is time-invariant so followers 7 and 8 collide at t=0.37 s. This implies MAS collective motion practically terminates at t=0.37 although it can be theoretically continued if containment control requirements are satisfied.

The problem illustrated above occurs because followers' communication weights are not consistent with agents' positions at initial time $t_0=0\,\mathrm{s}$. This paper directly addresses this issue by defining agent coordination as a continuum deformation acquired via local communication. Because continuum deformation is a nonsingular mapping, no two particles occupy the same position during transformation. Therefore, interagent collision avoidance can be guaranteed. Because interagent distances can be significantly expanded or contracted, the MAS can also maneuver in obstacle environments including traversal through narrow channels. In a continuum deformation coordination, follower communication weights are required to be consistent with agents' initial positions. This requirement will not be restricting so long as the following conditions are satisfied.

- 1) Every follower arbitrarily communicates with three inneighbor agents forming an enclosing triangle.
- 2) Interagent communication is defined by a directed graph containing a spanning tree.
- 3) 2-D continuum deformation coordination is guided by $N_L \geq 3$ leaders.

Therefore, consistency of communication weights with agents' initial positions does not necessarily limit applicability and scalability of a continuum deformation coordination.

Remark 1: In [22], it is shown that continuum deformation coordination can be acquired by followers through local communication if each follower is allowed to communicate with three or more in-neighbor agents. However, communication weights are not unique when each follower communicates with more than three in-neighbor agents in 2-D continuum deformation coordination. In this paper, we assume that each follower communicates with three in-neighbor agents only for the sake of uniqueness of the communication weights.

III. PROBLEM STATEMENT

This paper studies continuum deformation of a quadcopter team in 3-D motion space. The quadcopter team consists of N_L leader quadcopters and $N-N_L$ followers. Leaders move independently and their reference trajectories are defined by a homogeneous transformation as given in (5). Followers communicate with local in-neighbor agents to acquire continuum deformation coordination in a decentralized fashion. An ex-

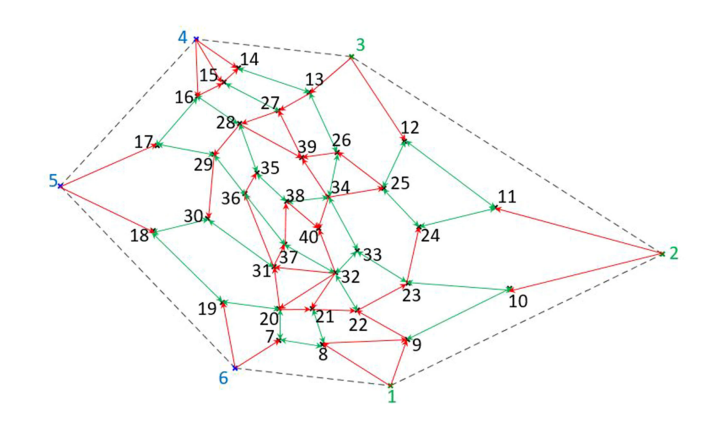


Fig. 2. Example directed communication topology in a quadcopter team consisting of $N_L=6$ leaders and 34 followers. Primary leaders, secondary leaders, and followers are shown by green, blue, and black nodes, respectively. Unidirectional and bidirectional communications are distinguished by red one-sided arrows and green double-sided arrows, respectively.

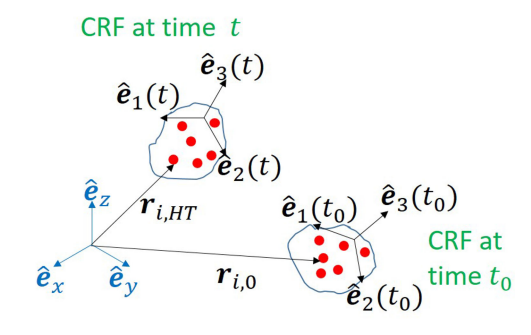


Fig. 3. 2-D continuum deformation in a 3-D motion space. $\hat{\mathbf{e}}_x$, $\hat{\mathbf{e}}_y$, and $\hat{\mathbf{e}}_z$ are the ground coordinate system bases. Reference frame orthogonal bases are denoted as $\hat{\mathbf{e}}_1(t)$, $\hat{\mathbf{e}}_2(t)$, and $\hat{\mathbf{e}}_3(t)$. The CRF can freely translate and rotate in a 3-D motion space, allowing the quadcopter team to deform inside the CRF.

ample quadcopter team communication topology is shown in Fig. 2. The paper improves quadcopter team maneuverability by formulating collective motion as a continuum deformation over a *moving frame*. This is achieved by treating members of a quadcopter team as particles of a moving deformable body or continuum. It is desired that the continuum frame has an arbitrary translation and rotation in 3-D motion space, while the quadcopter team can significantly deform inside the continuum frame. A schematic of a 2-D continuum deformation in a 3-D motion space is shown in Fig. 3. Continuum deformation over a moving frame is defined by 1) rigid body rotation and translation and 2) quadcopter team deformation relative to the frame.

The main objective of this paper is to guarantee quadcopter containment and interagent collision avoidance in a large-scale continuum deformation. To ensure quadcopter containment, this paper defines a convex prism containing all quadcopters at all times t. It will be proven that follower quadcopters that are inside the containment prism at initial time t_0 will remain inside the containment prism at any time $t > t_0$. Therefore, obstacle collision avoidance is guaranteed if the boundary surfaces of the containment prism do not hit obstacles in the motion space.

Because interagent distances can significantly change in a continuum deformation, interagent collision avoidance must be guaranteed. To ensure interagent collision avoidance, we need to obtain the Jacobian matrix $\mathbf{Q}(t) \in \mathbb{R}^{3 \times 3}$ and the rigid body displacement $\mathbf{d}(t) \in \mathbb{R}^{3 \times 1}$ given leader trajectories $\mathbf{r}_1(t)$, $\mathbf{r}_2(t)$, and $\mathbf{r}_3(t)$ for any time t. This paper addresses the challenging problem of identifying \mathbf{Q} and \mathbf{d} when the quadcopter team deforms over a moving frame. The constraints ensuring interagent collision avoidance are obtained in Section VI.

IV. QUADCOPTER TEAM CONTINUUM DEFORMATION OVER A MOVING FRAME

Suppose a quadcopter team is tasked with following a collective motion profile guided by $N_L \geq 3$ leaders. Leaders 1, 2, and 3 uniquely define an MAS continuum reference frame (CRF) and are called *primary leaders*. Remaining leaders (leaders 4,..., N_L) are called *secondary leaders*. All leaders' global desired positions can be defined per (5); however, elements of \mathbf{Q} and \mathbf{d} are defined based on the primary leaders' trajectories.

A. CRF Definition and Evolution

The MAS CRF is defined by a triangle with vertices occupied by leaders 1, 2, and 3. This CRF can arbitrarily deform and rotate while primary leaders' positions satisfy the following rank condition:

$$\forall t \geq t_0, \quad \text{Rank} \begin{bmatrix} \mathbf{r}_{2,HT} - \mathbf{r}_{1,HT} & \mathbf{r}_{3,HT} - \mathbf{r}_{1,HT} \end{bmatrix} = 2.$$
 (7)

This rank condition ensures that the CRF forms a 2-D convex hull at any time t. Given the global desired positions of primary leaders 1, 2, 3, the CRF bases are defined by

$$\hat{\mathbf{e}}_{1} = \frac{\mathbf{r}_{2,HT} - \mathbf{r}_{1,HT}}{\|\mathbf{r}_{2,HT} - \mathbf{r}_{1,HT}\|}, \, \hat{\mathbf{e}}_{2} = \frac{\mathbf{r}_{3,HT} - \mathbf{r}_{B_{1},HT}}{\|\mathbf{r}_{3,HT} - \mathbf{r}_{B_{1},HT}\|},$$

$$\hat{\mathbf{e}}_3 = \hat{\mathbf{e}}_1 \times \hat{\mathbf{e}}_2$$
.

The unit vectors $\hat{\mathbf{e}}_1$, $\hat{\mathbf{e}}_2$, $\hat{\mathbf{e}}_3$ are mutually orthogonal. Note that $\mathbf{r}_{3,HT} - \mathbf{r}_{B_1,HT}$ is perpendicular to $\mathbf{r}_{2,HT} - \mathbf{r}_{1,HT}$, where $\mathbf{r}_{B_1,HT}$ is located on the line passing through $\mathbf{r}_{1,HT}$ and $\mathbf{r}_{2,HT}$ as shown in Fig. 4. Therefore

$$\mathbf{r}_{B_1,HT} = \mathbf{r}_{1,HT} + \rho_1 \left(\mathbf{r}_{2,HT} - \mathbf{r}_{1,HT} \right) \tag{8a}$$

$$\rho_1 = \frac{(\mathbf{r}_{2,HT} - \mathbf{r}_{1,HT}) \cdot (\mathbf{r}_{3,HT} - \mathbf{r}_{1,HT})}{(\mathbf{r}_{2,HT} - \mathbf{r}_{1,HT}) \cdot (\mathbf{r}_{2,HT} - \mathbf{r}_{1,HT})}.$$
 (8b)

1) Continuum Deformation With a Virtual Leader: It is assumed that there is no deformation along the $\hat{\mathbf{e}}_3$ axis at any time $t \geq t_0$. Without loss of generality, the position of virtual leader N+1, given by

$$\forall t > t_0, \qquad \mathbf{r}_{N+1|HT}(t) = \mathbf{r}_{1|HT}(t) + \Xi \hat{\mathbf{e}}_3(t)$$
 (9)

is along positive $\hat{\mathbf{e}}_3$ and $\Xi > 0$ is an arbitrary number. Then, leaders 1, 2, 3, and N+1 form a tetrahedron at any $t \geq t_0$, and

Rank
$$([\mathbf{r}_{2,HT} - \mathbf{r}_{1,HT} \quad \mathbf{r}_{3,HT} - \mathbf{r}_{1,HT} \quad \mathbf{r}_{N+1,HT} - \mathbf{r}_{1,HT}])$$

= 3. (10)

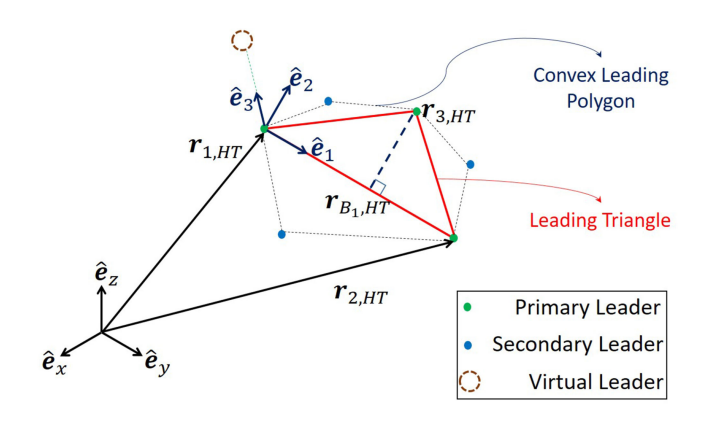


Fig. 4. Graphical representation of the MAS CRF, ground coordinate unit basis vector $(\hat{\mathbf{e}}_x, \hat{\mathbf{e}}_y, \hat{\mathbf{e}}_z)$; leader global desired positions $\mathbf{r}_{1,HT}$, $\mathbf{r}_{2,HT}$, $\mathbf{r}_{3,HT}$; and the CRF unit basis vector $(\hat{\mathbf{e}}_1, \hat{\mathbf{e}}_2, \hat{\mathbf{e}}_3)$, and $\mathbf{r}_{B_1,HT}$.

We define

$$t \ge t_0, \qquad \mathbf{P}(t) = \left[egin{array}{cccc} x_1(t) & y_1(t) & z_1(t) \ x_2(t) & y_2(t) & z_2(t) \ x_3(t) & y_3(t) & z_3(t) \ x_{N+1}(t) & y_{N+1}(t) & z_{N+1}(t) \end{array}
ight].$$

The elements of **Q** and **d** can then be uniquely related to $\mathbf{r}_{1,HT}$, $\mathbf{r}_{2,HT}$, $\mathbf{r}_{3,HT}$, and $\mathbf{r}_{N+1,HT}$ by

$$\begin{bmatrix} \operatorname{vec} \left(\mathbf{Q}^{T} \left(t \right) \right) \\ \mathbf{d} \left(t \right) \end{bmatrix} = \begin{bmatrix} \mathbf{I}_{3} \otimes \mathbf{P} \left(t_{0} \right) & \mathbf{I}_{3} \otimes \mathbf{1}_{4} \end{bmatrix}^{-1} \operatorname{vec} \left(\mathbf{P} \left(t \right) \right).$$
(11)

 $\mathbf{I}_3 \in \mathbb{R}^{3 \times 3}$ is an identity matrix and $\mathbf{1}_4 \in \mathbb{R}^{4 \times 1}$ is a one vector. α -parameters: $\tilde{\mathbf{r}}_{i,HT} = \mathbf{r}_{i,HT} - \mathbf{r}_{1,HT}$ denotes the relative global desired position of leader i (i=1,2,3) expressed with respect to the CRF. The relative global desired position $\tilde{\mathbf{r}}_{i,HT} = (x_{i,HT} - x_{1,HT})\hat{\mathbf{e}}_x + (y_{i,HT} - y_{1,HT})\hat{\mathbf{e}}_y + (z_{i,HT} - z_{1,HT})\hat{\mathbf{e}}_z$ can be expressed as $\tilde{\mathbf{r}}_{i,HT} = \gamma_i\hat{\mathbf{e}}_1(t) + \beta_i\hat{\mathbf{e}}_2(t)$ (i=1,2,3), where γ_i and β_i can be uniquely related to $x_{i,HT}, y_{i,HT}$, and $z_{i,HT}$ by

$$\begin{bmatrix} \hat{\mathbf{e}}_1 & \hat{\mathbf{e}}_2 & \hat{\mathbf{e}}_3 \end{bmatrix} \begin{bmatrix} \gamma_i \\ \beta_i \\ 0 \end{bmatrix} = \begin{bmatrix} x_{i,HT} - x_{1,HT} \\ y_{i,HT} - y_{1,HT} \\ z_{i,HT} - z_{1,HT} \end{bmatrix}.$$
(12)

For 2-D homogeneous transformation in 3-D motion space, quadcopter's $\mathbf{r}_{i,HT}(t)$ ($i \in \mathcal{V}_F$) desired position is given by

$$i \in \mathcal{V}_F, \qquad \mathbf{r}_{i,HT}(t) = \alpha_{i,1}\mathbf{r}_{1,HT} + \alpha_{i,2}\mathbf{r}_{2,HT} + \alpha_{i,3}\mathbf{r}_{3,HT}$$

$$(13)$$

where $\alpha_{i,k}$ is unique and obtained from solving the following three linear algebraic equations:

$$\begin{bmatrix} \gamma_{1}(t_{0}) & \gamma_{2}(t_{0}) & \gamma_{3}(t_{0}) \\ \beta_{1}(t_{0}) & \beta_{2}(t_{0}) & \beta_{3}(t_{0}) \\ 1 & 1 & 1 \end{bmatrix} \begin{bmatrix} \alpha_{i,1} \\ \alpha_{i,2} \\ \alpha_{i,3} \end{bmatrix} = \begin{bmatrix} \gamma_{i,HT}(t_{0}) \\ \beta_{i,HT}(t_{0}) \\ 1 \end{bmatrix}. \quad (14)$$

B. Continuum Deformation Acquisition

Without loss of generality, this paper assumes that the desired trajectory of leader quadcopter i, between initial position $\mathbf{r}_{i,0}$ and target destination $\mathbf{r}_{i,q}$, is given by

$$i=1,2,3, t \in [t_0, t_0 + T_{\text{total}}], \quad \mathbf{r}_{d,i} = (\mathbf{r}_{i,g} - \mathbf{r}_{i,0}) \, s_i + \mathbf{r}_{i,0}$$

where $s_i(t) = \sum_{l=0}^{5} \zeta_{i,l} t^{5-l}$ (i=1,2,3), subject to $s_i(t_0) = 0$, $s_i(t_0 + T_{\text{total}}) = 1$, $\dot{s}_i(t_0) = \dot{s}_i(t_0 + T_{\text{total}}) = 0$, and $\ddot{s}_i(t_0) = 0$ $\ddot{s}_i(t_0 + T_{\text{total}}) = 0$. Coefficients $\zeta_{i,0}$ through $\zeta_{i,5}$ are the solution of the following set of linear algebraic equations:

$$\begin{bmatrix} T_{\rm total}^5 & T_{\rm total}^4 & T_{\rm total}^3 & T_{\rm total}^2 & T_{\rm total} & 1\\ 0 & 0 & 0 & 0 & 0 & 1\\ 5T_{\rm total}^4 & 4T_{\rm total}^3 & 3T_{\rm total}^2 & 2T_{\rm total} & 1 & 0\\ 0 & 0 & 0 & 0 & 1 & 0\\ 20T_{\rm total}^3 & 12T_{\rm total}^2 & 6T_{\rm total} & 2 & 0 & 0\\ 0 & 0 & 0 & 2 & 0 & 0 \end{bmatrix} \begin{bmatrix} \zeta_{0,i} \\ \zeta_{1,i} \\ \zeta_{2,i} \\ \zeta_{3,i} \\ \zeta_{4,i} \\ \zeta_{5,i} \end{bmatrix}$$

$$= \begin{bmatrix} 1 \\ 0 \\ 0 \\ 0 \\ 0 \\ 0 \end{bmatrix}. \tag{16}$$

Followers acquire a desired homogeneous transformation through local communication. We assume that quadcopter $i \in \mathcal{V}_F$ updates its position based on the positions of three inneighbor quadcopters i_1 , i_2 , i_3 ($\mathcal{N}_i = \{i_1, i_2, i_3\}, \forall i \in \mathcal{V}_F$), where followers' in-neighbor agents are specified by a directed graph. Fig. 2 shows a sample graph used for a 2-D local communication continuum deformation. It is assumed that the quadcopters' initial positions satisfy the following rank condition at

$$\begin{bmatrix} \mathbf{r}_{i_2,HT}(t_0) - \mathbf{r}_{i_1,HT}(t_0) & \mathbf{r}_{i_3,HT}(t_0) - \mathbf{r}_{i_1,HT}(t_0) \end{bmatrix} = 2.$$
(17)

Communication weights are obtained from

$$\begin{bmatrix} \gamma_{i_1}(t_0) & \gamma_{i_2}(t_0) & \gamma_{i_3}(t_0) \\ \beta_{i_1}(t_0) & \beta_{i_2}(t_0) & \beta_{i_3}(t_0) \\ 1 & 1 & 1 \end{bmatrix} \begin{bmatrix} w_{i,i_1} \\ w_{i,i_2} \\ w_{i,i_3} \end{bmatrix} = \begin{bmatrix} \gamma_i(t_0) \\ \beta_i(t_0) \\ 1 \end{bmatrix}. \quad (18)$$

Note that $w_{i,i_1} + w_{i,i_2} + w_{i,i_3} = 1 \ (\forall i \in \mathcal{V}_F).$

Remark 2: It is beneficial to ensure that follower communication weights are all positive. This can enhance the follower convergence rate to desired positions defined by a homogeneous transformation. When communication weights are all positive, then 1) each follower $i \in \mathcal{V}_F$ will be located inside the communication triangle i defined by in-neighbor agents i_1 , i_2 , and i_3 , and 2) followers are all inside the leading polygon. Therefore, follower i is closer to the centroid of communication triangle iand MAS evolution stability can be improved. Mathematically speaking, the magnitude of the closest eigenvalue of matrix L from the imaginary axis is increased; therefore, the convergence

rate is increased. Notice that the closest eigenvalue of matrix L to the imaginary axis is negative and real [21].

Assumption 1: Each follower $i \in \mathcal{V}_F$ is located inside the communication triangle whose vertices are occupied by inneighbor quadcopters $i_1, i_2, i_3 \in \mathcal{N}_i$. Therefore, the followers' communication weights are all positive.

Assumption 2: Digraph \mathcal{G} defining interagent communication among quadcopters contains a spanning tree, and position information flows from leaders to every quadcopter $i \in \mathcal{V}_F$.

Assumption 3: If $N_L > 3$, the FL-communication matrix Ω from (2) is partitioned as follows:

$$\mathbf{\Omega} = \begin{bmatrix} \mathbf{\Omega}_{pf} & \mathbf{\Omega}_{sf} \end{bmatrix} \tag{19}$$

where $\Omega_{pf} \in \mathbb{R}^{(N-N_L) imes 3}$ and $\Omega_{sf} \in \mathbb{R}^{(N-N_L) imes (N_L-3)}$. Note that subscripts are defined such that p indicates the set of primary leaders, s indicates the set of secondary leaders, and f indicates followers.

Assumption 4: If $N_L > 3$, we define

$$\mathbf{\Omega}_{ps} = \begin{bmatrix} \alpha_{4,1} & \alpha_{4,2} & \alpha_{4,3} \\ \vdots & \vdots & \vdots \\ \alpha_{N_L,1} & \alpha_{N_L,2} & \alpha_{N_L,3} \end{bmatrix} \in \mathbb{R}^{(N_L - 3) \times 3}$$
 (20)

where each α -parameter $\alpha_{i,j}$ $(i = 4, ..., N_L \text{ and } j = 1, 2, 3)$ is computed from (14) given the initial position of secondary leader $i \in \mathcal{V}_L \setminus \{1, 2, 3\}$ and the primary leaders' positions. Because the leading polygon is strongly convex at the initial time t_0 , the secondary leaders are all outside the leading triangle. Therefore, each secondary leader has at least one negative communication weight and one positive communication weight.

Theorem 1: We define

$$\mathbf{z}_{m,HT,p}\left(t
ight) = egin{bmatrix} m_{1,HT} \ m_{2,HT} \ m_{3,HT} \end{bmatrix}, \, \mathbf{z}_{m,HT,s}\left(t
ight) = egin{bmatrix} m_{4,HT} \ dots \ m_{N_L,HT} \end{bmatrix}$$

$$\mathbf{z}_{m,HT,f}\left(t
ight) = egin{bmatrix} m_{N_L+1,HT} \ dots \ m_{N,HT} \ \end{bmatrix}$$

as components $m \in \{x, y, z\}$ for the primary leaders, secondary leaders, and followers. If follower communication weights and secondary leader α -parameters are consistent with initial quadcopter positions and assigned using (18), then

$$\begin{bmatrix} \mathbf{\Omega}_{ps} & -\mathbf{I} & \mathbf{0} \\ \mathbf{\Omega}_{pf} & \mathbf{\Omega}_{sf} & \mathbf{L} \end{bmatrix} \begin{bmatrix} \mathbf{z}_{m,HT,p} (t_0) \\ \mathbf{z}_{m,HT,s} (t_0) \\ \mathbf{z}_{m,HT,f} (t_0) \end{bmatrix} = \begin{bmatrix} \mathbf{0} \\ \mathbf{0} \\ \mathbf{0} \end{bmatrix}. \tag{21}$$

Theorem 2: If follower communication weights w_{i,i_1}, w_{i,i_2} , w_{i,i_3} satisfy (18), and the communication graph \mathcal{G} contains a spanning tree, the following statements are true.

1) The matrix $\mathbf{L} \in \mathbb{R}^{(N-N_L)\times (N-N_L)}$ is Hurwitz.

2) The matrix

$$\mathbf{W}_{L} = -\mathbf{L}^{-1}\mathbf{\Omega} = -\mathbf{L}^{-1}\left(\mathbf{\Omega}_{pf} + \mathbf{\Omega}_{sf}\mathbf{\Omega}_{pf}\right)$$
$$\in \mathbb{R}^{(N-N_{L})\times 3}$$
(22)

is one-sum row, i.e., the sum of the row elements is 1 for all rows of matrix \mathbf{W}_L .

3) The entry of row $i-N_L$ and column j of \mathbf{W}_L is equal to $\alpha_{i,j}$ ($i \in \mathcal{V}_F$, $j \in \{1,2,3\}$), where $\alpha_{i,j}$ is determined by (14) given initial positions of the three leaders and follower $i \in \mathcal{V}_F$.

Corollary (Global Desired Configuration): The followers' global desired positions, defined by a homogeneous transformation, are given by

$$\forall t \ge t_0, \ m = x, y, z, \qquad \mathbf{z}_{m,HT,f} = \mathbf{W}_L \mathbf{z}_{m,HT,p}. \tag{23}$$

V. QUADCOPTER TEAM COLLECTIVE DYNAMICS

Given the quadcopter dynamics modeled in Appendix A, the quadcopter team collective dynamics can be expressed as

$$\dot{\mathbf{z}}_{MQS} = \mathbf{A}_{SYS} \mathbf{z}_{MQS} + \mathbf{B}_{SYS} \mathbf{u}_{MQS}$$
 (24)

where

$$\mathbf{A}_{\mathrm{SYS}} = \mathbf{I}_3 \otimes egin{bmatrix} \mathbf{0}_N & \mathbf{I}_N & \mathbf{0}_N & \mathbf{0}_N \ \mathbf{0}_N & \mathbf{0}_N & \mathbf{I}_N & \mathbf{0}_N \ \mathbf{0}_N & \mathbf{0}_N & \mathbf{0}_N & \mathbf{I}_N \ k_4 \mathbf{W} & k_3 \mathbf{W} & -k_2 \mathbf{I}_N & -k_1 \mathbf{I}_N \end{bmatrix}$$

 $\mathbf{B}_{\mathrm{SYS}} =$

$$egin{pmatrix} \left(\mathbf{I}_3 \otimes \begin{bmatrix} \mathbf{0}_{N_L imes N} & \mathbf{0}_{N_L imes N} & \mathbf{0}_{N_L imes N} & \mathbf{I}_{N_L} & \mathbf{0}_{N_L imes (N-N_L)} \end{bmatrix}
ight)^T$$

" \otimes " is the Kronecker product symbol, $\mathbf{0}_{N_L \times N} \in \mathbb{R}^{N_L \times N}$ and $\mathbf{0}_{N_L \times (N-N_L)} \in \mathbb{R}^{N_L \times (N-N_L)}$ are zero-entry matrices, and $\mathbf{I}_3 \in \mathbb{R}^{3 \times 3}$, $\mathbf{I}_{N_L} \in \mathbb{R}^{N_L \times N_L}$, $\mathbf{I}_N \in \mathbb{R}^{N \times N}$ are identity matrices. In addition

$$\mathbf{z}_{\text{MQS}} = \begin{bmatrix} \mathbf{z}_x^T & \cdots & \ddot{\mathbf{z}}_x^T & \mathbf{z}_y^T & \cdots & \ddot{\mathbf{z}}_y^T & \mathbf{z}_z^T & \cdots & \ddot{\mathbf{z}}_z^T \end{bmatrix}^T$$

$$\in \mathbb{R}^{12N \times 1}$$

is the quadcopter team state vector given by

$$\mathbf{z}_{x} = [\mathbf{z}_{x,l}^{T} \, \mathbf{z}_{x,f}^{T}]^{T}, \, \mathbf{z}_{x,l} = [x_{1} \, \cdots \, x_{N_{L}}]^{T},$$

$$\mathbf{z}_{x,f} = [x_{N_{L}+1} \, \cdots \, x_{N}]^{T}$$

$$\mathbf{z}_{y} = [\mathbf{z}_{y,l}^{T} \, \mathbf{z}_{y,f}^{T}]^{T}, \, \mathbf{z}_{y,l} = [y_{1} \, \cdots \, y_{N_{L}}]^{T},$$

$$\mathbf{z}_{y,f} = [y_{N_{L}+1} \, \cdots \, y_{N}]^{T}$$

$$\mathbf{z}_{z} = [\mathbf{z}_{z,l}^{T} \, \mathbf{z}_{z,f}^{T}]^{T}, \, \mathbf{z}_{z,l} = [z_{1} \, \cdots \, z_{N_{L}}]^{T},$$

$$\mathbf{z}_{z,f} = [z_{N_{L}+1} \, \cdots \, z_{N}]^{T}.$$

We define

$$\mathbf{z}_{m,HT}\left(t\right) = \begin{bmatrix} \mathbf{z}_{m,HT,l}\left(t\right) \\ \mathbf{z}_{m,HT,f}\left(t\right) \end{bmatrix}$$

with (m = x, y, z), $t \ge t_0$, $\mathbf{z}_{m,HT,l} = [m_{1,HT} \cdots m_{N_L,HT}]^T$, and $\mathbf{z}_{m,HT,f} = [m_{N_L+1,HT} \cdots m_{N,HT}]^T$. $\mathbf{u}_{\mathrm{MQS}}$ is then

given by

$$\mathbf{u}_{\text{MQS}} = \sum_{j=0}^{4} k_j \frac{\mathrm{d}^{4-j}}{\mathrm{d}t^{4-j}} \left(\begin{bmatrix} \mathbf{z}_{x,HT,l} \\ \mathbf{z}_{y,HT,l} \\ \mathbf{z}_{z,HT,l} \end{bmatrix} \right)$$
(25)

where $k_0 = 1$. Note that **W** was previously defined in (1).

Remark 3: Matrix **W** is Hurwitz (see Theorem 2). Control gains k_1 through k_4 are selected such that the roots of the quadcopter team collective characteristic equation

$$CH(s) = |s\mathbf{I} - \mathbf{A}_{SYS}| = 0 \tag{26}$$

are all located in the open left-half s-plane, where $\mathbf{I} \in \mathbb{R}^{12N \times 12N}$ is the identity matrix.

A. Collective Error Dynamics

Let $\tilde{\mathbf{z}}_m$ (m = x, y, z) be the difference between actual and desired quadcopter positions

$$\tilde{\mathbf{z}}_{m} = \begin{bmatrix} \tilde{\mathbf{z}}_{m,l} \\ \cdots \\ \tilde{\mathbf{z}}_{m,f} \end{bmatrix} = \begin{bmatrix} \mathbf{z}_{m,l} - \mathbf{z}_{m,HT,l} \\ \cdots \\ \tilde{\mathbf{z}}_{m,f} - \mathbf{z}_{m,HT,f} \end{bmatrix}. \tag{27}$$

Then, the MQS collective dynamics (24) can be rewritten as

$$\sum_{j=0}^{2} k_{j} \frac{\mathrm{d}^{4-j}}{\mathrm{d}t^{4-j}} \left(\begin{bmatrix} \mathbf{z}_{x} \\ \mathbf{z}_{y} \\ \mathbf{z}_{z} \end{bmatrix} \right) + \sum_{j=3}^{4} k_{j} \left(\mathbf{I}_{3} \otimes \begin{bmatrix} -\mathbf{I} & \mathbf{0} \\ \mathbf{\Omega} & \mathbf{L} \end{bmatrix} \right) \\
\times \frac{\mathrm{d}^{4-j}}{\mathrm{d}t^{4-j}} \left(\begin{bmatrix} \mathbf{z}_{x} \\ \mathbf{z}_{y} \\ \mathbf{z}_{z} \end{bmatrix} \right) \\
= \sum_{j=0}^{4} k_{j} \left(\mathbf{I}_{3} \otimes \begin{bmatrix} \mathbf{I}_{N_{L}} \\ \mathbf{0}_{(N-N_{L}) \times N_{L}} \end{bmatrix} \right) \frac{\mathrm{d}^{4-j}}{\mathrm{d}t^{4-j}} \left(\begin{bmatrix} \mathbf{z}_{x,HT,l} \\ \mathbf{z}_{y,HT,l} \\ \mathbf{z}_{z,HT,l} \end{bmatrix} \right).$$

Let $\Omega = -\mathbf{L}(-\mathbf{L}^{-1}\Omega) = -\mathbf{L}\mathbf{W}_L$ be substituted in (28) where \mathbf{W}_L was previously defined in (22). Then

$$\Omega \mathbf{z}_{x,l} = -\mathbf{L} \mathbf{W}_L(\tilde{\mathbf{z}}_{x,l} + \mathbf{z}_{x,HT,l}) = \Omega \tilde{\mathbf{z}}_{x,l} - \mathbf{L} \mathbf{z}_{x,HT,f}$$
(29a)

$$\Omega \mathbf{z}_{v,l} = -\mathbf{L} \mathbf{W}_L (\tilde{\mathbf{z}}_{v,l} + \mathbf{z}_{v,HT,l}) = \Omega \tilde{\mathbf{z}}_{v,l} - \mathbf{L} \mathbf{z}_{v,HT,f}$$
 (29b)

$$\mathbf{\Omega}\mathbf{z}_{z,l} = -\mathbf{L}\mathbf{W}_{L}(\tilde{\mathbf{z}}_{z,l} + \mathbf{z}_{z,HT,l}) = \mathbf{\Omega}\tilde{\mathbf{z}}_{z,l} - \mathbf{L}\mathbf{z}_{z,HT,f}.$$
(29c)

Therefore

$$\sum_{j=0}^{2} \left(\frac{\mathrm{d}^{4-j}}{\mathrm{d}t^{4}} \left(\begin{bmatrix} \tilde{\mathbf{z}}_{x} \\ \tilde{\mathbf{z}}_{y} \\ \tilde{\mathbf{z}}_{z} \end{bmatrix} \right) \right) + \sum_{j=3}^{4} k_{j} \left(\mathbf{I}_{3} \otimes \mathbf{W} \right) \frac{\mathrm{d}^{4-j}}{\mathrm{d}t^{4-j}}$$

$$\times \left(\begin{bmatrix} \mathbf{z}_{x,HT,l} \\ \mathbf{z}_{y,HT,l} \\ \mathbf{z}_{z,HT,l} \end{bmatrix} \right) = \mathbf{E}_{Q}$$
(30)

where

$$\mathbf{E}_{\mathbf{Q}} = \sum_{j=0}^{2} k_{j} \left(\mathbf{I}_{3} \otimes \begin{bmatrix} \mathbf{0} \\ \mathbf{W}_{L} \end{bmatrix} \right) \frac{\mathrm{d}^{4-j}}{\mathrm{d}t^{4-j}} \left(\begin{bmatrix} \tilde{\mathbf{z}}_{x,HT,l} \\ \tilde{\mathbf{z}}_{y,HT,l} \\ \tilde{\mathbf{z}}_{z,HT,l} \end{bmatrix} \right) \in \mathbb{R}^{3N \times 1}.$$
(31)

Defining

 $\mathbf{z}_{\text{MQS},HT}$

$$= [\mathbf{z}_{x,HT}^T \cdots \mathbf{\ddot{z}}_{x,HT}^T \mathbf{z}_{y,HT}^T \cdots \mathbf{\ddot{z}}_{y,HT}^T \mathbf{z}_{z,HT}^T \cdots \mathbf{\ddot{z}}_{z,HT}^T]^T$$

$$\in \mathbb{R}^{12N \times 1}$$

and $\tilde{\mathbf{z}}_{MQS} = \mathbf{z}_{MQS} - \mathbf{z}_{MQS,HT}$, the error collective dynamics (30) can be expressed by the following state-space form:

$$\dot{\tilde{z}}_{MQS} = \mathbf{A}_{SYS}\tilde{\mathbf{z}}_{MQS} + (\mathbf{I}_3 \otimes \begin{bmatrix} \mathbf{0}_{N \times 3N} & \mathbf{I}_N \end{bmatrix})^T \mathbf{E}_{Q}. \quad (32)$$

The solution of the error dynamics in (32) is given by

$$\mathbf{\tilde{z}}_{MQS} = \mathbf{C}_{SYS} \left[e^{\mathbf{A}_{SYS} t} \mathbf{\tilde{z}}_{MQS}(0) + \int_{0}^{t} e^{\mathbf{A}_{SYS} \tau} \right] \times \left(\mathbf{I}_{3} \otimes \begin{bmatrix} \mathbf{0}_{3N \times N} \\ \mathbf{I}_{N} \end{bmatrix} \right) \mathbf{E}_{Q} d\tau \tag{33}$$

where $\mathbf{C}_{\mathrm{SYS}} = \mathbf{I}_3 \otimes [\mathbf{I}_N \, \mathbf{0} \, \mathbf{0} \, \mathbf{0}]$. $\mathbf{E}_{\mathrm{Q}}(\frac{t}{T_{\mathrm{total}}})$ is a vector [see (15)], where T_{total} is the travel time between initial and target formations. T_{total} is selected sufficiently large that the deviation of every quadcopter i is less than upper bound δ

$$\forall i \in \mathcal{V}_F, \qquad \|\mathbf{r}_i - \mathbf{r}_{i,HT}\| \le \delta.$$
 (34)

VI. SAFE AND SCALABLE COORDINATION CONDITIONS

This section assigns safety conditions ensuring interagent collision avoidance and quadcopter containment in a large-scale continuum deformation coordination.

A. Safe Continuum Deformation Coordination

Using polar decomposition, the homogeneous transformation Jacobian matrix can be expressed as $\mathbf{Q} = \mathbf{R}_D \mathbf{U}_D$, where rotation matrix \mathbf{R}_D is orthogonal and matrix \mathbf{U}_D is a positive definite. This is because \mathbf{R}_D is orthogonal $\mathbf{U}_D^2 = \mathbf{Q}^T \mathbf{Q}$.

Note that $\lambda_i = \lambda_i(\mathbf{U}_D) = \lambda_i(\sqrt{\mathbf{Q}^T\mathbf{Q}}) > 0$ if leaders do not align during the continuum deformation. Because the leading polygon is normal to the vector $\hat{\mathbf{e}}_3$ at any time t, $\lambda_3 = 1$. The paper assumes that $0 \le \lambda_1 \le \lambda_2$.

Let D_B be the minimum separation distance between all leader and follower quadcopter pairs, and let D_S denote the minimum distance of any follower quadcopter from the boundary of the leading triangle at initial time t_0 (see Fig. 5). It is assumed that each quadcopter is enclosed by a ball with radius ϵ . Given D_S , D_B , and ϵ , we define

$$\delta_{\max} = \min \left\{ \frac{1}{2} (D_B - 2\epsilon), (D_S - \epsilon) \right\}$$
 (35)

as the upper-bound for the error signal

$$\forall t \ge t_0 \quad \forall i, \qquad \delta = \sup \|\mathbf{r}_i(t) - \mathbf{r}_{i,HT}(t)\|.$$
 (36)

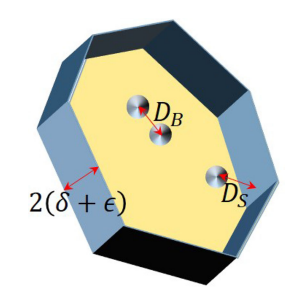


Fig. 5. Containment prism schematic showing minimum separation D_B and boundary distance D_S at initial time t_0 .

Because δ_{\max} is assigned based on D_B and D_S using (35), both containment guarantees and interagent collision avoidance are assured if every quadcopter satisfies inequality (34) and $\delta \leq \delta_{\max}$ for all times t.

Theorem 3: We assume

$$\lambda_{\text{CD.min}} \le \lambda_1 \left(\mathbf{U}_D \right)$$
 (37)

where

$$\lambda_{\rm CD,min} = \frac{\delta + \epsilon}{\delta_{\rm max} + \epsilon} = \frac{\delta/\delta_{\rm max} + \epsilon/\delta_{\rm max}}{1 + \epsilon/\delta_{\rm max}}$$
(38)

 λ_1 is the smallest eigenvalue of the matrix \mathbf{U}_D , ϵ is the quadcopter body size, and δ_{\max} and δ are assigned by (35) and (36), respectively. Then, the following statements are true: 1) interagent collision avoidance is assured and 2) quadcopters remain inside a containment prism with two polygonal bases¹ and N_L rectangular surfaces between the two bases. Note that rectangular boundary surfaces all have the same height $2(\delta + \epsilon)$ (see Fig. 5).

B. Scalable Continuum Deformation Coordination

We call continuum deformation coordination scalable if both inequalities (safety conditions) (34) and (37) are satisfied for a large value of N. Inequality (34) is a temporal constraint that can be satisfied by choosing a sufficiently large travel time $T_{\rm total}$. This property is demonstrated in Fig. 11 of the simulation section. Inequality (37) imposes a geometric constraint on quadcopter continuum deformation by assigning a lower bound on the eigenvalues of matrix \mathbf{U}_D given deviation upper bound δ , quadcopter size ϵ , and $\delta_{\rm max}$ assigned by (35).

Fig. 6 plots $\lambda_{\rm CD,min}$ versus $\epsilon/\delta_{\rm max}$ for different $\delta/\delta_{\rm max}$ ($\delta/\delta_{\rm max}=0,\ldots,0.9$). For large N, continuum deformation safety is guaranteed, if $\lambda_1({\bf U}_D)$ is greater than $\lambda_{\rm CD,min}$ at any time t given the upper bound δ , quadcopter size ϵ , and $\delta_{\rm max}$. Note that δ depends on quadcopter control performance as well as $T_{\rm total}$, that is, deviation upper bound δ decreases as $T_{\rm total}$ rises. $\lambda_{\rm CD,min}$ (lower limit for ${\bf U}_D$ eigenvalues), quadcopter size ϵ , and $\delta_{\rm max}$ must be appropriately selected such that safety is guaranteed in a large-scale team.

¹Bases of the containment prism are translated copies of the leading convex polygon and are equidistant from the leading convex polygon.

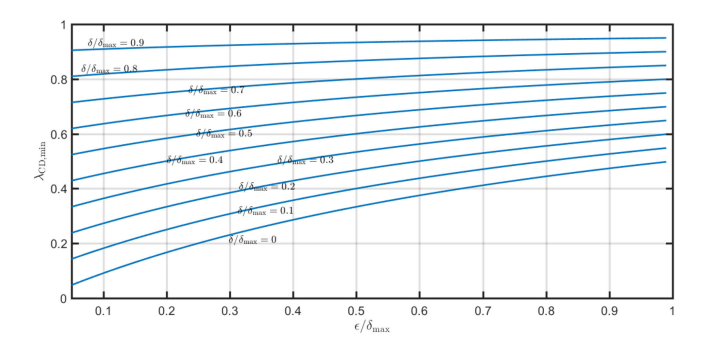


Fig. 6. $\lambda_{CD,m\,in}$ versus $\epsilon/\delta_{m\,ax}$ for $\delta/\delta_{m\,ax}=0,0.1,\ldots,0.9$.

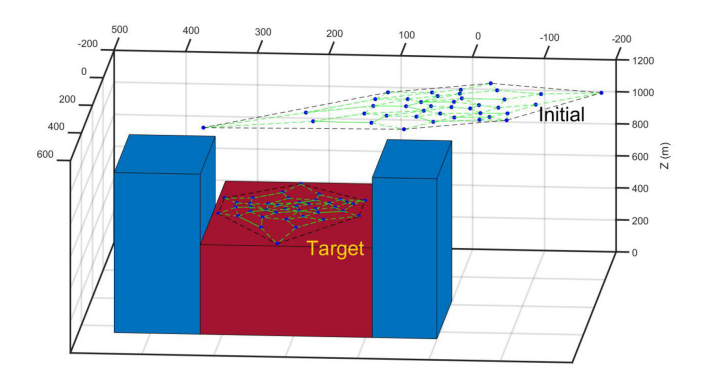


Fig. 7. Quadcopter team initial and target formations.

VII. SIMULATION RESULTS

We consider a quadcopter team consisting of 40 quadcopters in a collective descent scenario. Quadcopters 1, 2, 3 are primary leaders and quadcopters 4, 5, 6 are secondary leaders. The remaining quadcopters are followers. The quadcopter team is treated as a 2-D continuum deforming in a 3-D motion space. Quadcopter initial positions are shown in Fig. 7.

A. CRF Evolution

Given primary leaders' initial positions ($\mathbf{r}_{1,0} = 360\hat{\mathbf{e}}_x + 900\hat{\mathbf{e}}_z$, $\mathbf{r}_{2,0} = 72\hat{\mathbf{e}}_x + 108\hat{\mathbf{e}}_y + 1008\hat{\mathbf{e}}_z$, and $\mathbf{r}_{3,0} = 108\hat{\mathbf{e}}_x - 72\hat{\mathbf{e}}_y + 1080\hat{\mathbf{e}}_z$), the basis of the deformation plane is obtained from

$$\hat{\mathbf{e}}_1(t_0) = \frac{\mathbf{r}_{2,0} - \mathbf{r}_{1,0}}{\|\mathbf{r}_{2,0} - \mathbf{r}_{1,0}\|_2} = \begin{bmatrix} -0.8835 & 0.3313 & 0.3313 \end{bmatrix}^T$$

$$\hat{\mathbf{e}}_2(t_0) = \begin{bmatrix} -0.1280 & -0.8509 & 0.5096 \end{bmatrix}^T$$

$$\hat{\mathbf{e}}_3(t_0) = \begin{bmatrix} 0.4507 & 0.4078 & 0.7941 \end{bmatrix}^T.$$

The case study objective for the quadcopter team is to safely land on a podium inside a narrow passage as shown in Fig. 7. Leader goal (destination) states are located at $\mathbf{r}_{g,1} = \mathbf{r}_1(T_{\text{total}}) = 224\hat{\mathbf{e}}_x + 434\hat{\mathbf{e}}_y + 560\hat{\mathbf{e}}_z$, $\mathbf{r}_{g,2} = \mathbf{r}_2(T_{\text{total}}) = 126\hat{\mathbf{e}}_x + 224\hat{\mathbf{e}}_y + 560\hat{\mathbf{e}}_z$, and $\mathbf{r}_{g,3} = \mathbf{r}_3(T_{\text{total}}) = 322\hat{\mathbf{e}}_x + 224\hat{\mathbf{e}}_y + 560\hat{\mathbf{e}}_z$. Primary leader trajectories are assigned by (15). Given the primary leader trajectories, the elements of \mathbf{Q} and \mathbf{d} are computed using (11). Eigenvalues of matrix $\mathbf{U}_D = \sqrt{\mathbf{Q}^T\mathbf{Q}}$ can be plotted

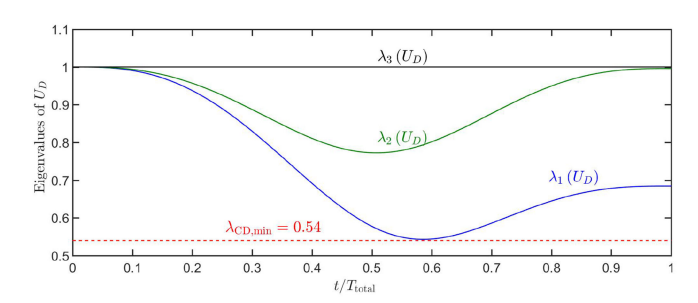


Fig. 8. Eigenvalues of pure deformation matrix U_D versus $\frac{t}{T_{\mathrm{total}}}$.

versus $\frac{t}{T_{\text{total}}}$ as shown in Fig. 8. Observe that $\lambda_{\text{CD,min}} = 0.54$ is the lower limit for the \mathbf{U}_D eigenvalues.

B. Secondary Leaders' Evolution:

Secondary leaders are initially positioned at $\mathbf{r}_{4,0}=-72\hat{\mathbf{e}}_x+117.6\hat{\mathbf{e}}_y+1084\hat{\mathbf{e}}_z,\quad \mathbf{r}_{5,0}=-198\hat{\mathbf{e}}_x+37\hat{\mathbf{e}}_y+1197\hat{\mathbf{e}}_z,\quad \text{and } \mathbf{r}_{6,0}=-36\hat{\mathbf{e}}_x-62\hat{\mathbf{e}}_y+1156\hat{\mathbf{e}}_z.$ Given $\mathbf{Q}(t,0)$ and $\mathbf{d}(t,0)$, computed by (11), the secondary leaders' positions at time t are given by

$$\forall t \ge 0, i = 4, 5, 6, \quad \mathbf{r}_{i,HT}(t) = \mathbf{Q}(t,0)\mathbf{r}_{i,0} + \mathbf{d}(t,0).$$

C. Collision Avoidance

Given leader positions, the eigenvalues of matrix \mathbf{U}_D are plotted versus time in Fig. 10. Note that one of the eigenvalues of the matrix \mathbf{U}_D is always 1. Furthermore, $\lambda_1(t)>0.50~(\forall t\geq 0)$; therefore, we choose $\lambda_{\mathrm{CD,min}}=0.54$ as the lower-limit of the eigenvalues of matrix \mathbf{U}_D . Observe that quadcopter 14 has a minimum distance $D_S=14.6168~\mathrm{m}$ from boundary 1–2 of the leading triangle at the initial time. In addition, quadcopters 14 and 15 are the closest quadcopters with minimum separation distance $D_B=19.2603~\mathrm{m}$ at the initial time. We assume that the ball B_a enclosing quadcopter i has radius $\epsilon=1.5~\mathrm{m}$ and center located at the centroid of quadcopter i. Using (35), $\delta_{\mathrm{max}}=\min\left\{\frac{1}{2}(D_B-2\epsilon),(D_S-\epsilon)\right\}=8.1302~\mathrm{m}$. Deviation upper bound δ is calculated from (38)

$$\delta = \lambda_{\rm CD,min} \left(\delta_{\rm max} + \epsilon \right) - \epsilon = 3.7003 \ {\rm m}.$$

Because $\delta > 0$, interagent collision avoidance can be assured by increasing the travel time Δt and choosing appropriate values for control gains k_1 through k_4 .

D. Continuum Deformation Acquisition

Follower quadcopters use the communication graph shown in Fig. 2 to acquire continuum deformation through local communication. Communication weights are consistent with agents' initial positions and assigned by using (18). Selecting $k_1=8$, $k_2=24$, $k_3=51.5625$, and $k_4=23.4375$, quadcopter team collective dynamics is stable; roots of the characteristic (26) are all placed in the open left-half s-plane. x,y, and z components of follower quadcopter 20 are plotted versus time in Fig. 9. The maximum deviation of all followers at any $t\geq 0$ is given by

$$E_{\max} = \max_{\forall i \in \mathcal{V}} (\|\mathbf{r}_i - \mathbf{r}_{i,HT}\|_{\infty})$$

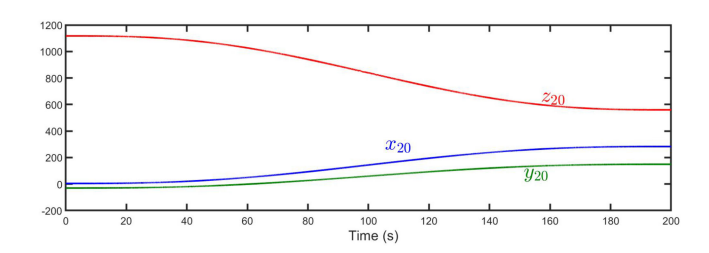


Fig. 9. Follower quadcopter 20 position versus time.

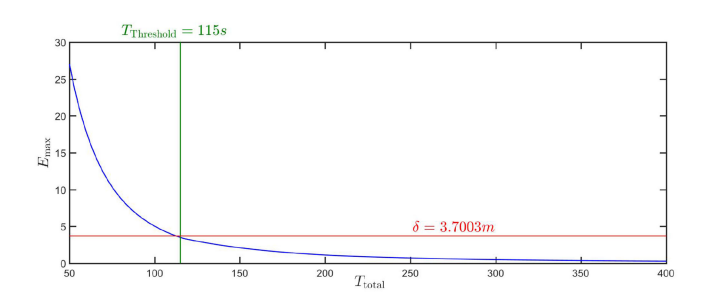


Fig. 10. Maximum follower deviation $E_{\rm m\,ax}$ for different values of travel times $t_{\rm total}$.

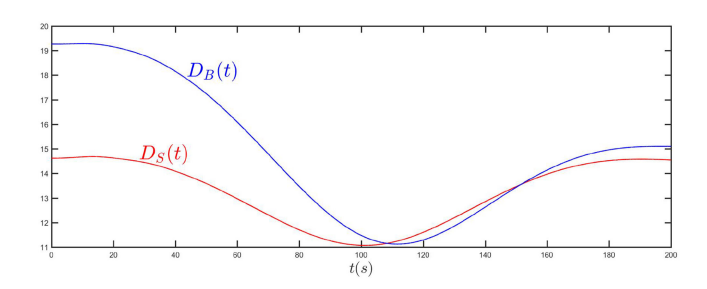


Fig. 11. Minimum separation distance $\mathcal{D}_{\mathcal{B}}$ and minimum boundary distance $\mathcal{D}_{\mathcal{S}}$ versus time.

where $\|\cdot\|_{\infty}$ denotes the infinity norm. In Fig. 10, E_{\max} is plotted for $50 \le T_{\rm total} \le 400$ s. It is seen that $E_{\max}(T_{\rm total}) \le 3.7003$ m, if $T_{\rm total} > T_{\rm Threshold} = 115$ s. Choosing $T_{\rm total} = 200$ s, minimum separation distance D_B and minimum distance D_S , from the lateral surfaces of the containment prism, are plotted versus time in Fig. 11. Because $D_S > 0$ at all t, no quadcopter leaves the containment prism. Also, no two quadcopters collide as $D_B > 0$ for all times t.

VIII. CONCLUSION

Continuum deformation for quadcopter team collective motion offers team scalability and substantial deformability within the group. This paper has extended continuum deformation from single/double integrator systems to multiquadcopter systems with six DOF nonlinear dynamics and moving reference frames based on moving leader positions. We showed that continuum deformation can be achieved with interagent collision-avoidance quadcopter containment guarantees. Scalability and safety of quadcopter team collective motion are demonstrated in a simulation scenario in which 40 quadcopters collectively land on a podium inside a narrow channel.

APPENDIX A QUADCOPTER MODEL

The actual position \mathbf{r}_i of every quadcopter is expressed with respect to an inertial coordinate system with unit bases $\hat{\mathbf{e}}_x$, $\hat{\mathbf{e}}_y$, and $\hat{\mathbf{e}}_z$ [see (3)]. However, it is more convenient to represent quadcopter rotational dynamics with respect to the body frame. Bases of the quadcopter body frame, denoted by $\hat{\mathbf{i}}_{b,i}$, $\hat{\mathbf{j}}_{b,i}$, and $\hat{\mathbf{k}}_{b,i}$, are related to $\hat{\mathbf{e}}_x$, $\hat{\mathbf{e}}_y$, and $\hat{\mathbf{e}}_z$ by

$$\begin{bmatrix}
\mathbf{i}_{b,i} \\
\hat{\mathbf{j}}_{b,i}
\end{bmatrix}$$

$$= \begin{bmatrix}
C_{\theta_i} C_{\psi_i} & C_{\theta_i} S_{\psi_i} & -S_{\theta_i} \\
S_{\phi_i} S_{\theta_i} C_{\psi_i} - C_{\phi_i} S_{\psi_i} & S_{\phi_i} S_{\theta_i} S_{\psi} + C_{\phi_i} C_{\psi_i} & S_{\phi_i} C_{\theta_i} \\
C_{\phi_i} S_{\theta_i} C_{\psi_i} + S_{\phi_i} S_{\psi_i} & C_{\phi_i} S_{\theta_i} S_{\psi_i} - S_{\phi_i} C_{\psi} & C_{\phi_i} C_{\theta_i}
\end{bmatrix}$$

$$\times \begin{bmatrix}
\hat{\mathbf{e}}_x \\
\hat{\mathbf{e}}_y \\
\hat{\mathbf{e}}_z
\end{bmatrix}. \tag{39}$$

In (39), $C_{(.)}$ and $S_{(.)}$ are abbreviations for $\cos(.)$ and $\sin(.)$, respectively. ϕ_i , θ_i , and ψ_i are roll, pitch, and yaw angles of quadcopter $i \in \mathcal{V}$. Throughout this paper, it is assumed that ψ_i is updated by $\ddot{\psi}_i = u_{\psi,i}$, where $\psi_i(0) = 0$, $\dot{\psi}_i(0) = 0$, and $u_{\psi,i}$ is updated by the stable dynamics

$$u_{\psi,i} = -k_{\phi,i}\psi_i - k_{\dot{\phi},i}\dot{\psi}_i. \tag{40}$$

If $k_{\phi,i}, k_{i,i} > 0$, $\psi_i(t) = 0$ for all t and (39) simplifies to

$$\begin{bmatrix} \hat{\mathbf{i}}_{b,i} \\ \hat{\mathbf{j}}_{b,i} \\ \hat{\mathbf{k}}_{b,i} \end{bmatrix} = \begin{bmatrix} \cos \theta_i & 0 & -\sin \theta_i \\ \sin \phi_i \sin \theta_i & \cos \phi_i & \sin \phi_i \cos \theta_i \\ \cos \phi_i \sin \theta_i & -\sin \phi_i & \cos \phi_i \cos \theta_i \end{bmatrix} \begin{bmatrix} \hat{\mathbf{e}}_1 \\ \hat{\mathbf{e}}_2 \\ \hat{\mathbf{e}}_3 \end{bmatrix}.$$
(41)

Define the (actual) position $\mathbf{r}_i = x_i \hat{\mathbf{e}}_x + y_i \hat{\mathbf{e}}_y + z_i \hat{\mathbf{e}}_z$, velocity $\mathbf{v}_i = v_{x,i} \hat{\mathbf{e}}_x + v_{y,i} \hat{\mathbf{e}}_y + v_{z,i} \hat{\mathbf{e}}_z$, the gravity g = 9.81 m/s², mass m_i , thrust force per mass $\bar{F}_{T,i} = \frac{F_{T,i}}{m_i}$, and control input $\mathbf{V}_i = [u_{T,i} \ u_{\phi_i} \ u_{\theta,i}]^T$. The dynamics of quadcopter $i \in \mathcal{V}$ is given by

$$\begin{cases} \dot{X}_{i} = \mathbf{f}(X_{i}) + \mathbf{g}(X_{i}) \mathbf{V}_{i} \\ h(X_{i}) = \mathbf{r}_{i} = \begin{bmatrix} x_{i} & y_{i} & z_{i} \end{bmatrix}^{T} \end{cases}$$
(42)

where $X_i = [x_i \ y_i \ z_i \ v_{x,i} \ v_{y,i} \ v_{z,i} \ \bar{F}_{T,i} \ \phi_i \ \theta_i \ \dot{\bar{F}}_{T,i} \ \dot{\phi}_i \ \dot{\theta}_i]^T \in \mathbb{R}^{12 \times 1}$ is the control state, h is the control output

$$\mathbf{g}^{T} = \begin{bmatrix} \mathbf{0} & \mathbf{I} \end{bmatrix} \in \mathbb{R}^{3 \times 12}$$

$$\mathbf{f} = [v_{x,i} \ v_{y,i} \ v_{z,i} \ f_{4} \ f_{5} \ f_{6} \ f_{7} \ f_{8} \ f_{9} \ 0 \ 0 \ 0]^{T}$$

$$f_{4} = \bar{F}_{T,i} \cos \phi_{i} \sin \theta_{i}$$

$$f_{5} = -\bar{F}_{T,i} \sin \phi_{i}$$

$$f_{6} = -g + \bar{F}_{T,i} \cos \phi_{i} \cos \theta_{i}$$

$$f_{j+3} = \dot{f}_{j}, \qquad j = 4, 5, 6.$$

Note that $\mathbf{0} \in \mathbb{R}^{3 \times 9}$ is the zero-entry matrix and $\mathbf{I} \in \mathbb{R}^{3 \times 3}$ is the identity matrix. The quadcopter dynamics given by (42) has a total relative degree $n_r = 12$. Using IO feedback linearization, quadcopter dynamics (42) can be converted to

$$\frac{\mathrm{d}^4 \mathbf{r}_i}{\mathrm{d}t^4} = \mathbf{U}_i \tag{43a}$$

$$\mathbf{U}_i = M_{T\phi\theta,i} \mathbf{V}_i + N_{T\phi\theta,i} \tag{43b}$$

where

 $M_{T\phi\theta,i}$

$$= \begin{bmatrix} \cos \phi_i \sin \theta_i & -\bar{F}_{T,i} \sin \phi_i \sin \theta_i & \bar{F}_{T,i} \cos \phi_i \cos \theta_i \\ -\sin \phi_i & -\bar{F}_{T,i} \cos \phi_i & 0 \\ \cos \phi_i \cos \theta_i & -\bar{F}_{T,i} \cos \theta_i \sin \phi_i & -\bar{F}_{T,i} \cos \phi_i \sin \theta_i \end{bmatrix}$$

$$\mathbf{N}_{T\phi\theta,i} = -2\dot{\bar{F}}_{T,i} \begin{bmatrix} \dot{\theta}_i \cos\phi_i \cos\theta_i - \dot{\phi}_i \sin\phi_i \sin\theta_i \\ -\dot{\phi}_i \cos\phi_i \\ -\dot{\theta}_i \cos\phi_i \sin\theta_i - \dot{\phi}_i \sin\phi_i \cos\theta_i \end{bmatrix}$$

$$-\bar{F}_{T,i} \begin{bmatrix} -\left(\dot{\theta}_i^2 + \dot{\phi}_i^2\right) \cos \phi_i \sin \theta_i - 2\dot{\theta}_i \dot{\phi}_i \sin \phi_i \cos \theta_i \\ \dot{\phi}_i^2 \sin \phi_i \\ -\left(\dot{\theta}_i^2 + \dot{\phi}_i^2\right) \cos \phi_i \cos \theta_i + 2\dot{\theta}_i \dot{\phi}_i \sin \phi_i \sin \theta_i \end{bmatrix}.$$

Define

$$\mathbf{P}_{d,i} = \sum_{j=0}^1 k_{4-j} \frac{\mathrm{d}^j \mathbf{r}_{d,i}}{\mathrm{d}t^j} \qquad \text{and} \qquad \mathbf{P}_i = \sum_{j=0}^4 k_{4-j} \frac{\mathrm{d}^j \mathbf{r}_i}{\mathrm{d}t^j}.$$

Choose the

$$\mathbf{U}_i = \mathbf{P}_{d,i} - \mathbf{P}_i \tag{44}$$

position of quadcopter i updated by the following fourth-order dynamics. By equating the right-hand sides of (43b) and (44), it is concluded that

$$\mathbf{U}_{i} = \frac{\mathrm{d}^{2} t}{\mathrm{d}t^{2}} \left(\begin{bmatrix} 0\\0\\-g \end{bmatrix} + \bar{F}_{T,i} \begin{bmatrix} \cos\phi_{i}\sin\theta_{i}\\-\sin\phi_{i}\\\cos\phi_{i}\cos\theta_{i} \end{bmatrix} \right). \tag{45}$$

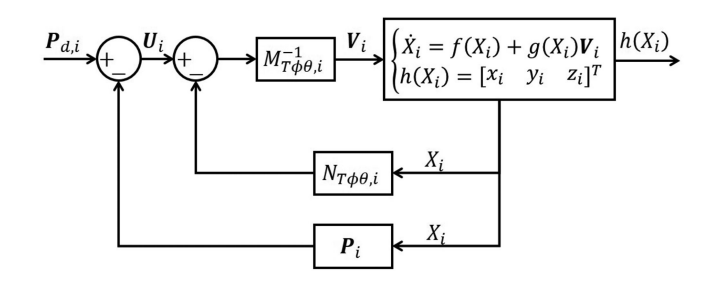
Equation (45) can be rewritten as

$$\mathbf{V}_{i} = \begin{bmatrix} u_{T,i} \\ u_{\phi,i} \\ u_{\theta,i} \end{bmatrix} = \begin{bmatrix} \ddot{F}_{T,i} \\ \ddot{\phi}_{i} \\ \ddot{\theta}_{i} \end{bmatrix} = M_{T\phi\theta,i}^{-1} \left(\mathbf{U}_{i} - \mathbf{N}_{T\phi\theta,i} \right). \quad (46) \qquad i \in \mathcal{V}_{L} \setminus \{1,2,3\}, \quad \sum_{j=1}^{3} \alpha_{i,j} \left(\mathbf{r}_{j,HT,0} - \mathbf{r}_{i,HT,0} \right) = 0. \quad (50)$$

Quadcopter *i*'s controller functionality is shown in Fig. 12.

APPENDIX B PROOFS OF THE THEOREMS

Proof of Theorem 1: The initial position of quadcopter $i \in \mathcal{V}$ can be expressed by $\mathbf{r}_{i,HT,0} = \mathbf{r}_{1,HT,0} + \gamma_i(t_0)\hat{\mathbf{e}}_1 +$ $\beta_i(t_0)\hat{\mathbf{e}}_2$. If communication weights are determined by (18),



Block diagram of the controller for quadcopter i.

then we can set up a weight matrix W using (2) where

$$\begin{bmatrix} \mathbf{\Omega}_{ps} & -\mathbf{I} & \mathbf{0} \\ \mathbf{\Omega}_{pf} & \mathbf{\Omega}_{sf} & \mathbf{L} \end{bmatrix} \begin{bmatrix} \gamma_1(t_0) & \cdots & \gamma_N(t_0) \end{bmatrix}^T = \mathbf{0}. \quad (47a)$$

$$\begin{bmatrix} \mathbf{\Omega}_{ps} & -\mathbf{I} & \mathbf{0} \\ \mathbf{\Omega}_{pf} & \mathbf{\Omega}_{sf} & \mathbf{L} \end{bmatrix} \begin{bmatrix} \beta_1(t_0) & \cdots & \beta_N(t_0) \end{bmatrix}^T = \mathbf{0}. \quad (47b)$$

Note that row i - 3 of (47) is equal to

$$\begin{cases} \sum_{j=1}^{3} \alpha_{i,j} \left(\gamma_{j} \left(t_{0} \right) - \gamma_{i} \left(t_{0} \right) \right) = 0 & i \in \mathcal{V}_{L} \setminus \{1, 2, 3\} \\ \sum_{j \in \mathcal{N}_{i}} w_{i,j} \left(\gamma_{j} \left(t_{0} \right) - \gamma_{i} \left(t_{0} \right) \right) = 0 & i \in \mathcal{V}_{F} \end{cases}$$

$$\tag{48a}$$

$$\begin{cases} \sum_{j=1}^{3} \alpha_{i,j} \left(\beta_{j} \left(t_{0} \right) - \beta_{i} \left(t_{0} \right) \right) = 0 & i \in \mathcal{V}_{L} \setminus \{1, 2, 3\} \\ \sum_{j \in \mathcal{N}_{i}} w_{i,j} \left(\beta_{j} \left(t_{0} \right) - \beta_{i} \left(t_{0} \right) \right) = 0 & i \in \mathcal{V}_{F}. \end{cases}$$

$$(48b)$$

$$i \in \mathcal{V}_{F}, \sum_{j \in \mathcal{N}_{i}} w_{i,j} \left(\mathbf{r}_{j,HT,0} - \mathbf{r}_{i,HT,0} \right)$$

$$= \mathbf{r}_{1} \left(\sum_{j \in \mathcal{N}_{i}} w_{i,j} - 1 \right)$$

$$+ \sum_{j \in \mathcal{N}_{i}} w_{i,j} \left[\left(\gamma_{j} \left(t_{0} \right) - \gamma_{i} \left(t_{0} \right) \right) \hat{\mathbf{e}}_{1} + \left(\beta_{j} \left(t_{0} \right) \right)$$

$$- \beta_{i} \left(t_{0} \right) \right) \hat{\mathbf{e}}_{2} \right]$$

$$= \sum_{j \in \mathcal{N}_{i}} w_{i,j} \left[\left(\gamma_{j} \left(t_{0} \right) - \gamma_{i} \left(t_{0} \right) \right) \hat{\mathbf{e}}_{1} + \left(\beta_{j} \left(t_{0} \right) \right)$$

$$- \beta_{i} \left(t_{0} \right) \right) \hat{\mathbf{e}}_{2} \right] = 0. \tag{49}$$

Similarly, it is concluded that

$$i \in \mathcal{V}_L \setminus \{1, 2, 3\}, \quad \sum_{j=1}^{3} \alpha_{i,j} \left(\mathbf{r}_{j,HT,0} - \mathbf{r}_{i,HT,0} \right) = 0.$$
 (50)

Consequently, (21) is satisfied when (49) and (50) are written in component-wise forms.

Proof of Theorem 2: There exist at least N_L followers communicating with N_L leaders. Because W is the zero-sum row, the sum of the elements in at least N_L rows of matrix **L** is negative; however, the sum of elements in the remaining rows of matrix L is zero. While diagonal elements of L are all -1, offdiagonal elements of L are non-negative. If the communication graph \mathcal{G} contains a spanning tree, matrix \mathbf{L} is irreducible and $-\mathbf{L}$ is a nonsingular M-matrix. Therefore, matrix $\mathbf{L} + \mathbf{I}$ has a spectral radius $\rho < 1$ and eigenvalues of matrix \mathbf{L} are all located inside a disk centered at $-1 + \mathrm{j}0$ and radius ρ [42]. From (21), we can write

$$\mathbf{z}_{m,HT,s}\left(t_{0}\right) = \mathbf{\Omega}_{ps}\mathbf{z}_{m,HT,p}\left(t_{0}\right) \tag{51a}$$

$$\mathbf{z}_{m,HT,f}\left(t_{0}\right) = -\mathbf{L}^{-1}\left(\mathbf{\Omega}_{pf}\mathbf{z}_{m,HT,p}\left(t_{0}\right) + \mathbf{\Omega}_{sf}\mathbf{z}_{m,HT,s}\left(t_{0}\right)\right)$$
(51b)

where $m \in \{x, y, z\}$. Substituting (51a) into (51b) yields $\mathbf{z}_{m,HT,f}(t_0) = \mathbf{W}_{fp}\mathbf{z}_{m,HT,p}(t_0)$, where $\mathbf{W}_{fp} = -\mathbf{L}^{-1}(\mathbf{\Omega}_{pf} + \mathbf{\Omega}_{sf}\mathbf{\Omega}_{pf})$. The entry of row $i - N_L$ and column j $(i \in \mathcal{V}_F, j \in \mathcal{V})$ entry of matrix \mathbf{W}_{fp} is equal to $\alpha_{i,j}$ from (14). Thus, \mathbf{W}_{fp} and \mathbf{W}_L are both one-sum row $(\mathbf{W}_{fp} = \mathbf{W}_L)$.

Proof of Theorem 3: Let m_1 and m_2 define two unique points of the leading triangle with minimum separation distance at initial time t_0 . If $0.5(D_B-2\epsilon) \leq (D_S-\epsilon)$, then m_1 and m_2 are assigned based on the two most closely spaced quadcopters at initial time t_0 . If $D_S-\epsilon < 0.5(D_B-2\epsilon)$, m_1 represents a quadcopter and m_2 is the closest point to m_1 on the boundary of the leading triangle. Consider (35), $\|\mathbf{r}_{m_1,0}-\mathbf{r}_{m_2,0}\|=\mu(\delta_{\max}+\epsilon)$, where $\mu=1$ if m_2 represents the closest point on the boundary of the leading triangle. Also, $\mu=2$, if m_2 represents a quadcopter inside the leading triangle with the closest separation distance. Interagent collision is avoided and no quadcopter leaves the leading triangle if

$$\mu = 1, 2, \|\mathbf{r}_{m_1}(t) - \mathbf{r}_{m_2}(t)\| \le \mu \left(\delta + \epsilon\right)$$
$$\le \|\mathbf{r}_{m_1, HT}(t) - \mathbf{r}_{m_2, HT}(t)\|.$$

Under a homogeneous transformation, $\mathbf{r}_{m_1,HT}$ and $\mathbf{r}_{m_2,HT}$ are updated by (5), where $\mathbf{r}_{m_1,0} = \mathbf{r}_{m_1,HT}(t_0)$ and $\mathbf{r}_{m_2,0} = \mathbf{r}_{m_2,HT}(t_0)$. Consequently

$$\|\mathbf{r}_{m_1,HT}(t) - \mathbf{r}_{m_2,HT}(t)\|^2 = (\mathbf{r}_{m_1,0} - \mathbf{r}_{m_2,0})^T$$

$$\times \mathbf{Q}^T \mathbf{Q} (\mathbf{r}_{m_1,0} - \mathbf{r}_{m_2,0})$$

$$= (\mathbf{r}_{m_1,0} - \mathbf{r}_{m_2,0})^T \mathbf{U}_D^2 (\mathbf{r}_{m_1,0} - \mathbf{r}_{m_2,0})$$

at any time t and, thus, $\lambda_{\mathrm{CD,mim}} = \frac{\delta + \epsilon}{\delta_{\mathrm{max}} + \epsilon} \leq \lambda_1 \leq \frac{\|\mathbf{r}_{m_1,HT}(t) - \mathbf{r}_{m_2,HT}(t)\|}{\|\mathbf{r}_{m_1,0} - \mathbf{r}_{m_2,0}\|}.$

REFERENCES

- X. Wang and G.-H. Yang, "Cooperative adaptive fault-tolerant tracking control for a class of multi-agent systems with actuator failures and mismatched parameter uncertainties," *IET Control Theory Appl.*, vol. 9, no. 8, pp. 1274–1284, 2015.
- [2] P. Zhao, S. Suryanarayanan, and M. Simoes, "An energy management system for building structures using a multi-agent decision-making control methodology," *IEEE Trans. Ind. Appl.*, vol. 49, no. 1, pp. 322–330, Jan/Feb. 2013.
- [3] C. H. Botts, J. C. Spall, and A. J. Newman, "Multi-agent surveillance and tracking using cyclic stochastic gradient," in *Proc. Amer. Control Conf.*, 2016, pp. 270–275.
- [4] D. Grether, "Extension of a multi-agent transport simulation for traffic signal control and air transport systems," Ph.D. dissertation, Tech. Univ. Berlin, Berlin, Germany, 2014.

- [5] X. Dong, Y. Zhou, Z. Ren, and Y. Zhong, "Time-varying formation tracking for second-order multi-agent systems subjected to switching topologies with application to quadrotor formation flying," *IEEE Trans. Ind. Electron.*, vol. 64, no. 6, pp. 5014–5024, Jun. 2016.
- [6] N. Goodall, B. Smith, and B. Park, "Traffic signal control with connected vehicles," *Trans. Res. Rec.: J. Trans. Res. Board*, vol. 2381, pp. 65–72, 2013
- [7] Y. Feng, K. L. Head, S. Khoshmagham, and M. Zamanipour, "A real-time adaptive signal control in a connected vehicle environment," *Transp. Res. Part C: Emerg. Technol.*, vol. 55, pp. 460–473, 2015.
- [8] C. B. Low and Q. San Ng, "A flexible virtual structure formation keeping control for fixed-wing UAVs," in *Proc. 9th IEEE Int. Conf. Control Autom.*, 2011, pp. 621–626.
- [9] W. Ren and R. W. Beard, "Decentralized scheme for spacecraft formation flying via the virtual structure approach," *J. Guid., Control, Dyn.*, vol. 27, no. 1, pp. 73–82, 2004.
- [10] W. Ren, R. W. Beard, and E. M. Atkins, "Information consensus in multivehicle cooperative control," *IEEE Control Syst.*, vol. 27, no. 2, pp. 71–82, Apr. 2007.
- [11] Y. Liu and Z. Geng, "Finite-time formation control for linear multiagent systems: A motion planning approach," Syst. Control Lett., vol. 85, pp. 54–60, 2015.
- [12] Y. Cao, W. Yu, W. Ren, and G. Chen, "An overview of recent progress in the study of distributed multi-agent coordination," *IEEE Trans. Ind. Inf.*, vol. 9, no. 1, pp. 427–438, Feb. 2013.
- [13] N. Rahbari-Asr, U. Ojha, Z. Zhang, and M.-Y. Chow, "Incremental welfare consensus algorithm for cooperative distributed generation/demand response in smart grid," *IEEE Trans. Smart Grid*, vol. 5, no. 6, pp. 2836– 2845, Nov. 2014.
- [14] S. E. Inzucchi et al., "Management of hyperglycemia in type 2 diabetes, 2015: A patient-centered approach: Update to a position statement of the american diabetes association and the european association for the study of diabetes," *Diabetes care*, vol. 38, no. 1, pp. 140–149, 2015.
- [15] S. Kar, G. Hug, J. Mohammadi, and J. M. Moura, "Distributed state estimation and energy management in smart grids: A consensus innovations approach," *IEEE J. Sel. Topics Signal Process.*, vol. 8, no. 6, pp. 1022–1038, Dec. 2014.
- [16] O. Hlinka, F. Hlawatsch, and P. M. Djuric, "Consensus-based distributed particle filtering with distributed proposal adaptation," *IEEE Trans. Signal Process.*, vol. 62, no. 12, pp. 3029–3041, Jun. 2014.
- [17] J. Qin, W. X. Zheng, H. Gao, Q. Ma, and W. Fu, "Containment control for second-order multiagent systems communicating over heterogeneous networks," *IEEE Trans. Neural Netw. Learn. Syst.*, vol. 28, no. 9, pp. 2143– 2155, Sep. 2017.
- [18] Z. Kan, J. Shea, and W. Dixon, "Leader-follower containment control over directed random graphs," *Automatica*, vol. 66, pp. 56–62, 2016.
- [19] Z. Li, Z. Duan, W. Ren, and G. Feng, "Containment control of linear multiagent systems with multiple leaders of bounded inputs using distributed continuous controllers," *Int. J. Robust Nonlinear Control*, vol. 25, no. 13, pp. 2101–2121, 2015.
- [20] H. Rastgoftar, Continuum Deformation of Multi-Agent Systems. Basel, Switzerland: Birkhäuser, 2016.
- [21] H. Rastgoftar, H. G. Kwatny, and E. M. Atkins, "Asymptotic tracking and robustness of MAS transitions under a new communication topology," *IEEE Trans. Autom. Sci. Eng.*, vol. 15, no. 1, pp. 16–32, Jan. 2018.
- [22] H. Rastgoftar and E. M. Atkins, "Continuum deformation of multi-agent systems under directed communication topologies," J. Dyn. Syst., Meas., Control, vol. 139, no. 1, 2017, Art. no. 011002.
- [23] N. H. Li and H. H. Liu, "Formation uav flight control using virtual structure and motion synchronization," in *Proc. Amer. Control Conf.*, 2008, pp. 1782–1787.
- [24] A. Essghaier, L. Beji, M. A. El Kamel, A. Abichou, and J. Lerbet, "Co-leaders and a flexible virtual structure based formation motion control," Int. J. Veh. Auton. Syst., vol. 9, nos. 1/2, pp. 108–125, 2011.
- [25] Z. Yang, J. Xiang, and Y. Li, "Distributed consensus based supply-demand balance algorithm for economic dispatch problem in a smart grid with switching graph," *IEEE Trans. Ind. Electron.*, vol. 64, no. 2, pp. 1600– 1610, Feb. 2017.
- [26] S. Rao and D. Ghose, "Sliding mode control-based autopilots for leader-less consensus of unmanned aerial vehicles," *IEEE Trans. Control Syst. Technol.*, vol. 22, no. 5, pp. 1964–1972, Sep. 2014.
- [27] W. Ren, "Distributed leaderless consensus algorithms for networked euler-lagrange systems," *Int. J. Control*, vol. 82, no. 11, pp. 2137–2149, 2009.

- [28] Q. Song, J. Cao, and W. Yu, "Second-order leader-following consensus of nonlinear multi-agent systems via pinning control," *Syst. Control Lett.*, vol. 59, no. 9, pp. 553–562, 2010.
- [29] L. Xu, H. Fan, Z. Dong, and W. Wang, "Robust consensus control for leader-following multi-agent system under switching topologies," in *Proc. Int. Conf. Cybern.*, Robust. Control, 2016, pp. 27–31.
- [30] F. Muñoz et al., "Adaptive consensus algorithms for real-time operation of multi-agent systems affected by switching network events," Int. J. Robust Nonlinear Control, vol. 27, no. 9, pp. 1566–1588, 2017.
- [31] G. Ferrari-Trecate, M. Egerstedt, A. Buffa, and M. Ji, "Laplacian sheep: A hybrid, stop-go policy for leader-based containment control," in *Proc. Int. Workshop Hybrid Syst.: Comput. Control*, 2006, pp. 212–226.
- [32] X. Wang, S. Li, and P. Shi, "Distributed finite-time containment control for double-integrator multiagent systems," *IEEE Trans. Cybern.*, vol. 44, no. 9, pp. 1518–1528, Sep. 2014.
- [33] G. Wen, Y. Zhao, Z. Duan, W. Yu, and G. Chen, "Containment of higher-order multi-leader multi-agent systems: A dynamic output approach," IEEE Trans. Autom. Control, vol. 61, no. 4, pp. 1135–1140, Apr. 2016.
- [34] Z. Li, W. Ren, X. Liu, and M. Fu, "Distributed containment control of multi-agent systems with general linear dynamics in the presence of multiple leaders," *Int. J. Robust Nonlinear Control*, vol. 23, no. 5, pp. 534–547, 2013.
- [35] X. He, Q. Wang, and W. Yu, "Finite-time containment control for secondorder multiagent systems under directed topology," *IEEE Trans. Circuits Syst. II, Exp. Briefs*, vol. 61, no. 8, pp. 619–623, Aug. 2014.
- [36] H. Su and M. Z. Chen, "Multi-agent containment control with input saturation on switching topologies," *IET Control Theory Appl.*, vol. 9, no. 3, pp. 399–409, 2015.
- [37] W. M. Lai, D. H. Rubin, D. Rubin, and E. Krempl, *Introduction to Continuum Mechanics*. Oxford, U.K.: Butterworth-Heinemann, 2009.
- [38] S. Zhao, "Affine formation maneuver control of multi-agent systems," IEEE Trans. Autom. Control, 2018.
- [39] S. Li and X. Wang, "Finite-time consensus and collision avoidance control algorithms for multiple auvs," *Automatica*, vol. 49, no. 11, pp. 3359–3367, 2013.
- [40] Y. Cao, D. Stuart, W. Ren, and Z. Meng, "Distributed containment control for multiple autonomous vehicles with double-integrator dynamics: Algorithms and experiments," *IEEE Trans. Control Syst. Technol.*, vol. 19, no. 4, pp. 929–938, Jul. 2011.
- [41] H. Rastgoftar, Continuum Deformation of Multi-Agent Systems. Berlin, Germany: Springer, 2016.
- [42] Z. Qu, Cooperative Control of Dynamical Systems: Applications to Autonomous Vehicles. New York, NY, USA: Springer, 2009.



Hossein Rastgoftar received the B.Sc. degree in mechanical engineering-thermo-fluids and the M.Sc. degree in mechanical systems and solid mechanics from Shiraz University, Shiraz, Iran, the M.Sc. degree in mechanical systems and solid mechanics from the University of Central Florida, Orlando, FL, USA, and the Ph.D. degree in mechanical engineering from Drexel University, Philadelphia, PA, USA, in 2015.

He is currently an Assistant Research Scientist with the University of Michigan, Ann Arbor,

MI, USA. His current research interests include dynamics and control, multiagent systems, human-cyber physical systems, Markov decision processes, and differential game theory.



Ella M. Atkins (SM'05) received the B.S. and M.S. degrees in aeronautics and astronautics from the Massachusetts Institute of Technology, Cambridge, MA, USA, and the M.S. and Ph.D. degrees in computer science and engineering from the University of Michigan, Ann Arbor, MI, USA.

She is currently a Professor of aerospace engineering with the University of Michigan, where she is also the Director of the Autonomous Aerospace Systems Laboratory and the Asso-

ciate Director of the Graduate Programs, Robotics Institute. Her research interests include aerospace system autonomy and safety.

Dr. Atkins is the Past Chair of the American Institute of Aeronautics and Astronautics Intelligent Systems Technical Committee. He has served on the National Academy.s Aeronautics and Space Engineering Board, the Institute for Defense Analysis Defense Science Studies Group, and the National Research Council Committee to develop an autonomy research agenda for civil aviation.



Dimitra Panagou (M'12) received the Diploma and Ph.D. degrees in mechanical engineering from the National Technical University of Athens, Athens, Greece, in 2006 and 2012, respectively.

Since 2014, she has been an Assistant Professor with the Department of Aerospace Engineering, University of Michigan, Ann Arbor, MI, USA. Prior to joining the University of Michigan, she was a Postdoctoral Research Associate with the Coordinated Science Laboratory, University of Illinois at Urbana-Champaign, from 2012 to

2014, a visiting research scholar with the GRASP Laboratory, University of Pennsylvania in 2010 and 2013, and a visiting research scholar with the Mechanical Engineering Department, University of Delaware, Newark, DE, USA, during Spring 2009. Her research interests include the fields of planning, coordination, and distributed control and estimation for complex systems, with applications in unmanned aerial systems, robotic networks, and autonomous multivehicle systems (ground, marine, aerial, and space).

Prof. Panagou was a recipient of the NASA 2016 Early Career Faculty Award and of the Air Force Office of Science Research 2017 Young Investigator Award.